# Molecular Dynamics Study of the Structures and Dynamics of the Iodine Molecules Confined in $AlPO_4$-11 Crystals

**J. M. Hu,[†] J. P. Zhai,[‡] F. M. Wu,[§] and Z. K. Tang*,[†]**

*Department of Physics and Institute of Nano Science and Technology, The Hong Kong University of Science and Technology, Clear Water Bay, Kowloon, Hong Kong, China, College of Electronic Science and Technology, Shenzhen University, Shenzhen 518060, China, and Institute of Condensed Matter Physics, Zhejiang Normal University, Jinhua, Zhejiang 321004, China*

*Received: August 13, 2010; Revised Manuscript Received: October 25, 2010*

Structural and dynamical properties of iodine molecules incorporated in one-dimensional elliptic channels of $AlPO_4$-11 (AEL) crystals were studied by means of molecular dynamics (MD) simulations. It was found that the iodine molecules in the AEL channels are restricted in the (101) planes with only two favorite orientations: lying along the channels and standing along the major axes of the ellipses, which are well consistent with the experimental observations. In addition, the iodine structures are largely dependent on the loading level: with the increase of loading, the iodine specimens change their structures accordingly from isolated molecules as in the gas phase to single molecular chains and molecular ribbon sheets. The molecular ribbon sheets are composed of equally distributed and parallel molecules as in the iodine crystals. The simulation results show that the standing iodine molecules in the AEL channels are well restricted due to both the appropriate size of ellipses and their alternation throughout the channels. They can diffuse along the channels only after overcoming the rotational barriers to become lying molecules, which indicate that the iodine molecules in the ribbon sheets can keep the configurations without rotational and translational motion. The confined iodine molecules with such structures and properties may be used to improve the accuracy of the frequency standards.



## 1. Introduction

Intercalating guest molecules into the matrix of the nanoporous crystals is a powerful method to localize and orientate molecules for molecular device applications.[1−4] Structural phase transitions,[5,6] electronic,[7] and magnetic properties[8,9] of the localized species have been intensively studied in recent years. Zeolite single crystals as well as carbon nanotubes are the widely used template materials to absorb and guide the size matched specimens.[10−13]

Spectroscopic properties of iodine molecules in the gas phase have been investigated in detail.[14−18] Because of its well-defined electron-vibrational structure and narrow absorption lines from the near-infrared down to the visible spectral range, gas-phase iodine was often considered as a reference for frequency stabilization.[19−21] In addition, the cell-based optical frequency standards of iodine molecules can offer a compact, simple, and less expensive system to make an optical molecular clock,[22] while the single ions and cold atoms require an elaborate system design. Thus, the iodine molecular frequency standards would greatly facilitate the application of frequency metrology both to precise experiments and to practical devices.

If the iodine molecules are localized and oriented by the nanoporous crystals without translational and rotational motions, the hyperfine electronic structures can be simplified to get sharper absorption lines than in the gas phase. Recently, we succeeded in incorporating iodine molecules into the channels of $AlPO_4$-11 (AEL) single crystals, which have the size nearly the same as the iodine molecules. It was found that due to the constraint, the iodine molecules are well aligned in the 10-ring elliptical channels of the AEL crystals and show polarized properties.[23,24] However, the specific information of the iodine molecules in the confined states, such as possible location, structures, and diffusion modes, is not yet clear.

In this work, we use molecular dynamics simulations[25,26] to investigate the structures as well as the dynamical properties of the iodine specimens in the AEL channels. We begin by analyzing the angular distribution of the iodine molecules and find that they are restricted in the (101) planes of the AEL crystals with their favorite orientations either lying along the channels or standing along the major axes of the ellipses. The structures of the iodine specimens are loading dependent, changing from gas phase to single molecular chains and molecular ribbon sheets with increasing loading level. The dynamics of the simulations show that the translational motion of the standing iodine is prohibited and the diffusion only happens when they are lying in the channels. Combining the structures and dynamical properties, we demonstrate that the iodine molecules in the ribbon sheets are parallel and equally distributed without rotational and translational motion. The iodine molecules in such confined states may be useful in improving the accuracy of the frequency standards.

## 2. Model and Simulation Details

AEL single crystal that has unidimensional and elliptic channels is a member of the aluminophosphate molecular sieves family. The single-crystal X-ray diffraction (XRD) shows that AEL crystal is of *Ima*2 space group symmetry with the lattice constants: $a = 13.519$ Å, $b = 18.652$ Å, and $c = 8.386$ Å, respectively. In the crystal, the aluminum (Al) and phosphor (P) atoms are alternatively linked through the oxygen (O) atoms. The size of the AEL elliptic channels alternates between wide

* Corresponding author. E-mail: phzktang@ust.hk.
[†] The Hong Kong University of Science and Technology.
[‡] Shenzhen University.
[§] Zhejiang Normal University.

10.1021/jp1076615 
Published on Web 11/16/2010

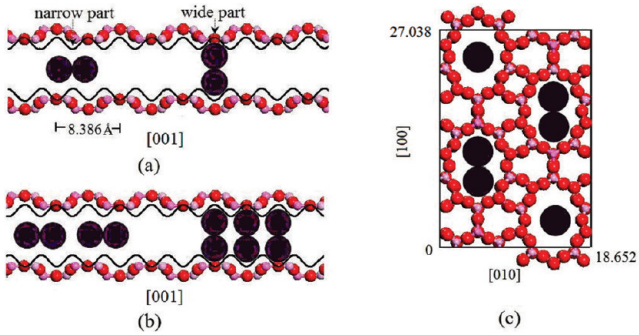


**Figure 1.** Schematic view of the AEL channels loaded with iodine molecules at (a) low and (b) high loading, respectively. The quasi-sinusoidal lines represent the potential energy at the end of the major axes of the ellipses. The purple molecules denote the iodine confined in the AEL channels. (c) The AEL crystal with iodine molecules projected in the (110) plane. The atoms in the box are used as the AEL framework in the simulation. Color coding for atoms is as follows: O, red; Al, light purple; P, pink.

parts and narrow parts with a period of $c/2$ throughout the channels, and the size of the narrow part is only 4.3 Å × 6.1 Å. The sketches of the AEL channels with the possible iodine structures and the AEL structures projected in (110) plane are shown in Figure 1, and the fractional coordinates of the AEL crystals we used are given in the Supporting Information.

In the simulations, the Buchart−Universal force field[27,28] was adopted. We described the AEL framework with Buchart force field and the iodine molecules with Universal force field. The parameters for the AEL−iodine interactions were derived from both force fields combination. The nonbonded interactions were modeled in terms of 12-6 Lennard-Jones potentials, given by

$$U(r_{ij}) = 4\varepsilon_{ij}\left[\left(\frac{\sigma_{ij}}{r_{ij}}\right)^{12} - \left(\frac{\sigma_{ij}}{r_{ij}}\right)^{6}\right] \quad (1)$$

where $\varepsilon_{ij}$ is the well-depth, $\sigma_{ij}$ is the site collision diameter, and $r_{ij}$ is the distance between the two interacting atoms $i$ and $j$. The Lorentz−Berthelot combination rules[29] have been used to compute the cross interaction parameters, as given by

$$\varepsilon_{ij} = \sqrt{\varepsilon_{ii} \times \varepsilon_{jj}} \quad (2)$$

$$\sigma_{ij} = (\sigma_{ii} + \sigma_{jj})/2 \quad (3)$$

No atomic partial charges were assigned. The bond stretch interactions of iodine molecules were treated using Morse potential.[30,31]

$$U(r) = D_e[1 - e^{-\alpha(r-r_e)}]^2 \quad (4)$$

where $D_e$ is the depth of the energy from the bottom of the well to bond dissociation, $r_e$ is the bond length in a given bound state, α controls the width of the well and can be described as $\alpha = (k_e/2D_e)^{1/2}$, where $k_e$ is the force constant at the minimum of the well. Detailed parameters are presented in Table 1. All the simulations were carried out in the canonical ensemble (NVT) at 300 K by Lammps.[32] The velocity-verlet algorithm with a time step of 0.5 fs was used to integrate the equation of motion. The simulation box was set to 2 × 1 × 10 unit cells, which have 4 channels with each channel 10 unit cells long.

**TABLE 1: Potential Parameters for the AEL Framework and the Iodine Molecules**

| atom type | ε (kcal/mol) | σ (Å) |
|---|---|---|
| I | 0.339 | 4.009 |
| O | 0.1648 | 2.940 |
| P | 0.0629 | 3.385 |
| Al | 0.0292 | 3.777 |

| bond type | $r_e$ (Å) | $D_e$ (eV) | α (Å$^{-1}$) |
|---|---|---|---|
| I−I | 2.66 | 1.544 | 1.867 |

Periodic boundary conditions were applied. A cutoff of 9.2 Å was set for nonbonded interactions. During the simulations, the AEL framework was considered to be fixed and defects free. At the beginning, the iodine molecules were randomly distributed in the channels with different loadings. The loadings in this work were between 2 and 20 iodine molecules per channel. For all cases, 4 ns equilibrium runs were performed first, followed by 6 ns productive runs for analyzing the statistical properties.

## 3. Results and Discussion

The configurations of the diatomic molecules confined in the nanoporous crystals can be described by analyzing the direction of the bonds in the channels. Figure 2 shows the angular distribution of the iodine molecules at the loading of 10 with the angles defined as in the inserts. In Figure 2a, the angle is defined from the bond of the iodine molecule to the (101) plane, while in Figure 2b, it is from the channel axis to the projection of the iodine bond in the (101) plane. It can be seen from Figure 2a that all of the angles are distributed between 0° and 15°, which means that the iodine molecules cannot rotate to the [010] direction due to the size restriction of the short axes of the ellipses. In Figure 2b, there are two predominant angular distributions at 0° and 90°, which correspond to the iodine molecules lying along the channels and standing along the major axes of the ellipses, respectively. Combining the two angular distributions, we conclude that the iodine molecules absorbed in the AEL channels are in fact confined in the (101) planes with only two preferred directions: lying along the channels and standing along the major axes of the ellipses. It suggests that the orientation of the iodine molecules can be controlled by manipulating the AEL crystals.

The confinement and orientation predilection of the iodine molecules in the AEL channels are well consistent with the polarized Raman results. The detailed sample preparation is available in the Supporting Information. The Raman spectra were measured at room temperature with a Jobin-Yvon T64000 micro-Raman spectrometer equipped with a liquid $N_2$ cooled CCD detector. The excitation laser line was 514.5 nm from an argon ion laser. Figure 3a−c shows three polarized Raman scattering configurations. To describe the polarization clearly, the AEL crystals were put in the $xyz$-coordinate and rotated along different axes. Figure 3d−f and g−i shows the corresponding Raman signals with the increase of the polarization angles at low and high loadings of iodine molecules, respectively. In Figure 3a, the incident excitation laser is polarized along the $z$-axis and propagates along the $\bar{y}$-axis. $\theta$ is the polarization angle from the $z$-axis to the crystal channel axis $c$. In the experiment, the polarization angle was turned by rotating the sample stage. As the polarized Raman spectra shown in Figure 3d, there are two highly polarized modes at 207 and 214 cm$^{-1}$. The intensity of the Raman signal at 207 cm$^{-1}$

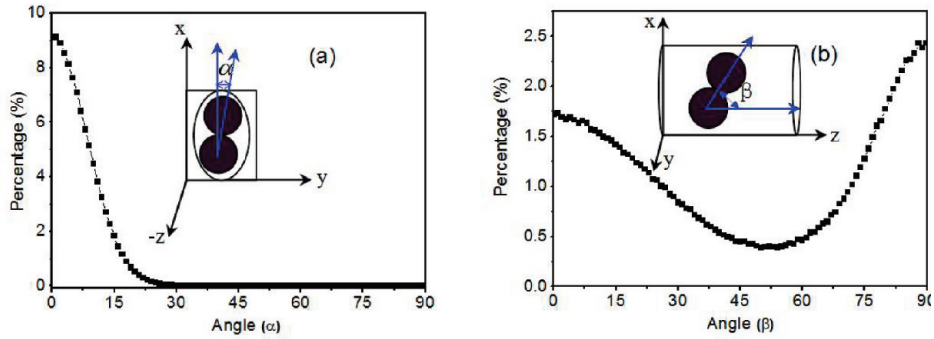


**Figure 2.** Angular distribution of the iodine molecules in the AEL channels at the loading of 10. (a) The angles between the iodine bonds and the (101) planes. (b) The angles between the channel axes and the projection of the iodine bonds in the (101) planes.

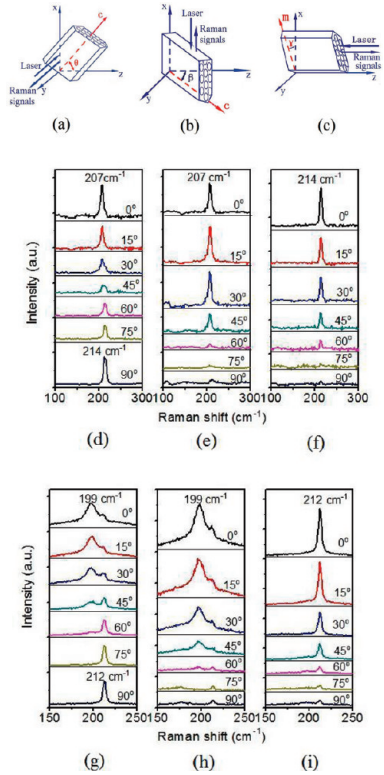


**Figure 3.** (a−c) Sketches of the polarized Raman scattering configurations. (d−f and g−i) The corresponding Raman signals measured from the above three configurations at low loadings and high loadings of iodine molecules, respectively.

decreases dramatically to zero, and that at 214 $cm^{-1}$ increases significantly with the increase of the polarization angles from $\theta = 0°$ to $\theta = 90°$. In Figure 3b, the incident laser is polarized along the $z$-axis and propagates along the $\bar{x}$-axis. $\beta$ is the polarization angle from the $z$-axis to the crystal channel axis $c$. The corresponding polarized Raman spectra in Figure 3e show that there is only one highly polarized mode at 207 $cm^{-1}$ whose intensity decreases dramatically to zero with the increase of the polarization angles from $\theta = 0°$ to $\theta = 90°$. In Figure 3c, the incident laser is polarized along the $x$-axis and propagates along the channel axis. $\gamma$ is the polarization angle from the $x$-axis to the major axis of the elliptical channel. The corresponding polarized Raman spectra in Figure 3f show that there is also only one Raman signal at 214 $cm^{-1}$ whose intensity decreases dramatically to zero with the increase of the polarization angle from $\gamma = 0°$ to $\gamma = 90°$. According to the Raman signals obtained from the Figure 3b,c scattering configurations, which have only one Raman signal in the direction of [001] and [100], we can conclude that the iodine molecules are strictly restricted in the (101) planes. These two Raman signals from the Figure 3a scattering configuration indicate that the iodine molecules have two predominant orientations. The Raman signal at 207 $cm^{-1}$ can be attributed to the iodine molecules lying along the AEL channels, while that at 214 $cm^{-1}$ originates from the iodine molecules standing along the major axes of the ellipses. The differences between the high loading and low loading of iodine molecules are that the Raman signal of 207 $cm^{-1}$ shifts to 199 $cm^{-1}$ and that of 214 $cm^{-1}$ shifts to 212 $cm^{-1}$ as the iodine molecules increase to high loading. The details of the experimental results can be found in refs 23 and 24.

To investigate the change of iodine structures at different loadings, the loading dependence of the angular distributions was studied, and the results are shown in Figure 4. The angles are defined in the same way as in the previous case. The loading range is from 2 to 20 iodine molecules per channel. It can be seen that the orientation predilections of the iodine molecules at different loadings are similar to those discussed in Figure 2. It means that the iodine molecules tend to lie along the channels or stand along the major axes of the ellipses in the (101) planes despite of loading. However, the ratio of the standing molecules to the lying molecules depends greatly on the loading. With increasing loading, more and more iodine molecules tend to gain the standing configurations.

At low loadings, the iodine molecules are separated away from each other in the channels, and the interactions between iodine molecules are negligible as in vapor phase. As the loadings increase, the interactions between the iodine molecules cannot be neglected in the arrangement, and the iodine molecules tend to form hand in hand single molecular chains, as shown in the left part of Figure 1b, and stand up to shoulder by shoulder molecular ribbon sheets, as shown in the right part of Figure 1b. As the loading continues to increase, the molecular ribbon sheets become the dominant structures. Thus, the percentage of standing iodine molecules increases remarkably. When the loading reaches 20, all the iodine molecules stand parallel in the AEL channels. The snapshots of the iodine structures projected in the (101) plane and (110) plane at three different loadings are shown in Figure 5.

The structural change can also be observed from the length of the single molecular chains and molecular ribbon sheets as a function of loading, as shown in Figure 6. The length of chains and ribbon sheets is defined as the number of molecules present in the structure that has more than two molecules with the same configuration and the separation of center-of-mass (CM) no larger than 11 and 6 Å, respectively. There are no chains or ribbon sheets at low loadings because of the large separation between iodine molecules. As the loading increases, both the molecular chains and the ribbon sheets start to appear and

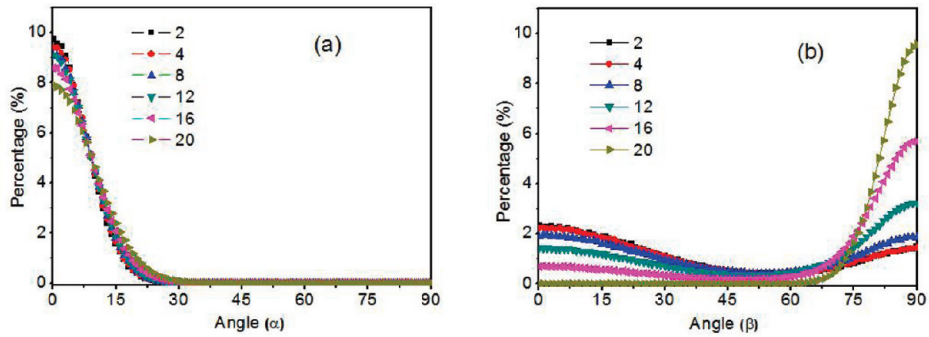


**Figure 4.** Angular distribution of iodine molecules in the AEL channels at different loadings. (a) The angles between the iodine bonds and the (101) planes. (b) The angles between the channel axes and the projection of the iodine bonds in the (101) planes.

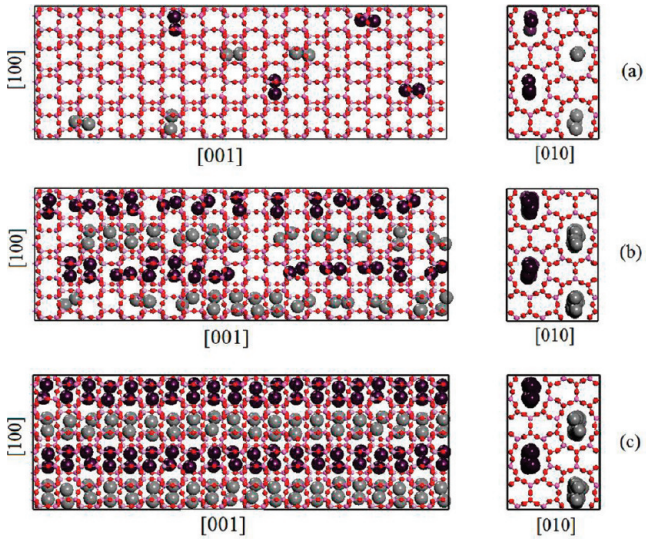


**Figure 5.** Snapshots of iodine structures confined in AEL channels at 300 K at the loadings of (a) 2, (b) 12, and (c) 20, respectively. The large diatomic molecules denote the iodine molecules, while the small atoms and lines denote the AEL framework. To clarify the channel effect, the iodine molecules in different channels are depicted in different colors. Views projected in the (101) plane (left) and (110) plane (right), respectively.

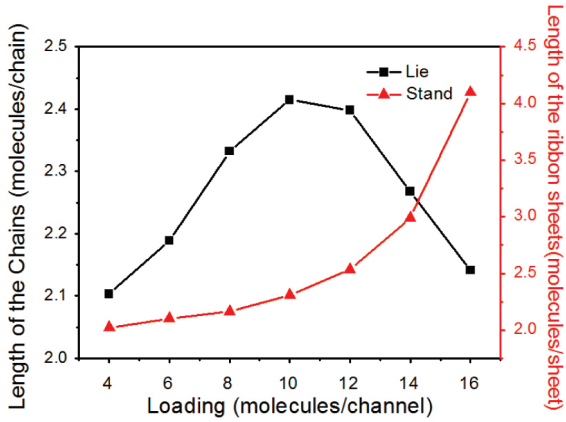


**Figure 6.** The length of the single molecular chains and ribbon sheets changes as a function of loading.

increase. With the continuous introduction of iodine molecules, the lying molecules tend to stand and the chains start to vanish, and the length of the ribbon sheets increases dramatically. At the saturated loading, the length of the ribbon sheet will be infinite long with the periodic boundary conditions, and the molecular ribbon sheets are the dominant structures.

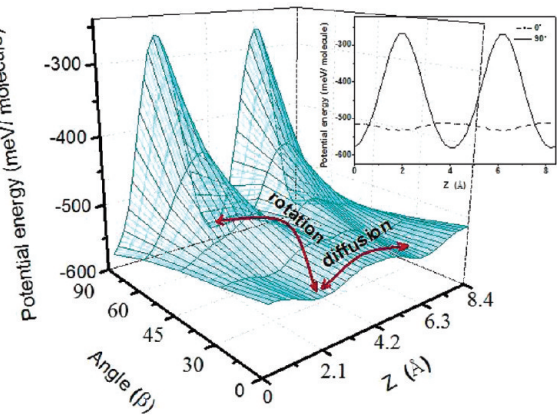


**Figure 7.** Potential energy surface of iodine molecules confined in the AEL channels with the angle from 0° to 90°. The arrows indicate the favorable pathways of the iodine molecules in the channels. The inset is the potential energy with the iodine molecules exactly standing and lying in the AEL channels.

The orientation predilection of the iodine can be explained by the potential energy surface of the iodine molecule in the channel with different configurations, as shown in figure 7. We can see that confined in the channels there are two stable states with the iodine molecules standing and lying in the channels as discussed before. The standing configuration is the most stable state, while the lying configuration is the metastable state. Between the two configurations, there is a rotational barrier, which makes the iodine molecules flip between the two configurations instead of rotating as continuously as in elliptical cylinder channels. The rotational barriers are the results of the construction of AEL channels, which is not only elliptical but also alternation between wide part and narrow part. To have a clear view, the potential energy profiles of the exactly standing and lying iodine molecules along the channels are given in the inset of Figure 7. The arrangement of the iodine molecules with different loadings originates from both the effective confinement of the AEL channels and the interactions between iodine molecules. Figure 7 shows that the potential energy is quite low, which means that the size of the AEL channels is exactly appropriate for iodine molecules. Because of the special confinement, the possible thermal fluctuation behaviors of the iodine molecules are the transition between the two configurations and diffusion along the channels when they are lying, which will be discussed later. The interactions between the neighboring iodine molecules increase the rotational barrier, which reduces the transition frequency between the two configurations and makes these configurations, especially the molecule ribbon sheets, more stable. Meanwhile, the standing iodine molecules hinder the diffusion of the lying molecules,

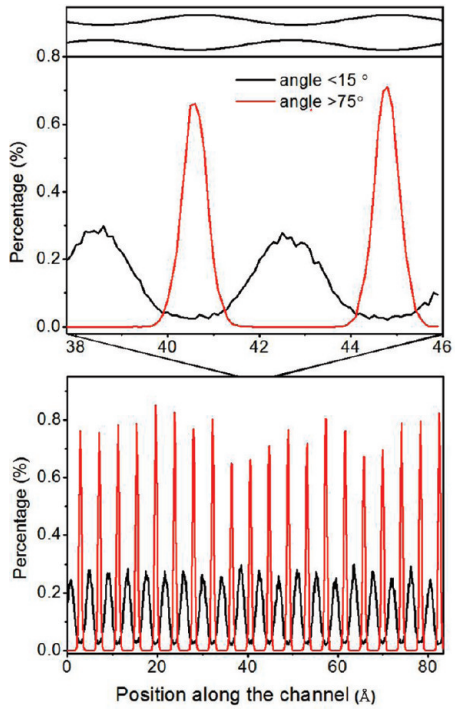


**Figure 8.** The density distribution of the center-of-mass of iodine molecules along the AEL channels with the iodine standing (angle >75°) and lying (angle <15°) in the channels, respectively. The top figure is the magnification of one part of the density distribution along the channel. The quasi-sinusoidal lines on top of the figure represent the schematic size of the channel.

and the molecular chains are formed in the confined states. Similar ordered structures due to the confinement have also been found, such as water molecule chains in carbon nanotubes.[33]

Although the structures such as single molecular chains and ribbon sheets are obtained, the specific locations of the iodine molecules in the AEL channels and the accurate distance between the arranged molecules are still unclear. Here, with the AEL framework as a reference, the density distribution of the CM of lying and standing iodine molecules at a loading of 10 is calculated, as shown in Figure 8. The lying and standing molecules are those with the angles, as defined in Figure 2b, smaller than 15° and larger than 75°, respectively. To have a clear view, one part of the density distribution is magnified with the schematic size of the AEL channel on top of the figure. It can be seen that the CM of the lying molecules prefers locating in narrow parts of the channels, while the standing iodine molecules are predominant in the wide parts. This means that due to the size modulation, the iodine atoms prefer to locate in the wide parts of the channels rather than in the narrow parts. For the lying molecules, the CM in the narrow parts means the two iodine atoms are located in the nearest neighboring wide parts with the bond getting across the narrow parts. For the standing iodine molecules, the two atoms are distributed in the same wide parts, as shown in Figure 1b.

Another obvious difference between the lying and standing molecules is that the distribution of standing molecules is much more concentrated than the lying molecules. The distance between each distribution peak of the standing molecules is exactly $c/2 = 4.19$ Å, which is close to the distance in iodine crystal.[34,35] Experimental observations have shown that the Raman peak of the iodine molecules standing in AEL channels (212 $cm^{-1}$) is much sharper than that of the lying molecules (199 $cm^{-1}$). In addition, the vibrational properties of the iodine

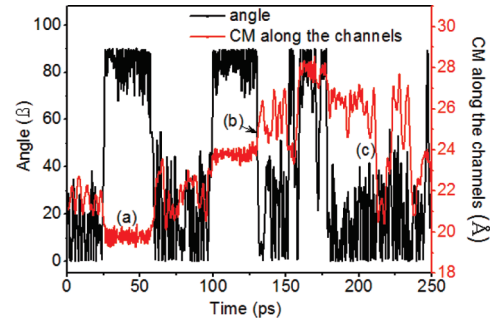


**Figure 9.** Angles and the corresponding center-of-mass of one iodine molecule along the channel as a function of simulation time at a loading of 10.

molecules in the ribbon sheets (the Raman signal at 212 $cm^{-1}$) are nearly the same as those of the iodine molecules in the gas phase (214.5 $cm^{-1}$),[36] which means that the interactions between the neighboring molecules in the ribbon sheets have little influence on the vibration properties. Contrarily, the Raman signal of the molecular chains shifts to 199 $cm^{-1}$ as a result of the interactions between the lying iodine molecules.

Combined with the potential energy surface of the iodine molecule in the channel, we can also see that when the iodine molecule is standing in the channel, the interactions are minimum at the wide parts ($z = 0$ and $z = 0.5c$) of the channel, and the potential energy increases sharply if it departs from the wide parts. Hence, the standing iodine molecules are exactly confined in the wide parts of the channels. In contrast, the interactions between the lying iodine molecules and AEL channels are much smoother with the minimum at the narrow parts of the channels. Thus, the lying iodine molecules prefer locating in the narrow parts, and the distribution is not as regular as the standing molecules due to its Brownian motion at 300 K.

To investigate the dynamics of the iodine molecules in the AEL channels, the angles (black curve) as well as the corresponding CM of one iodine molecule (red curve) along the channels (at a loading of 10) as a function of simulation time are presented together in Figure 9. It demonstrates that the iodine molecules have two states as mentioned before with the angle near 0° and 90°. When the iodine molecule is standing vertically in the channel, it will maintain its configuration for awhile until it overcomes the rotational barrier. Similarly, the lying molecule can also maintain its configuration with a small swage until it conquers the translational barrier or the rotational barrier again. Furthermore, there is no translational motion when the iodine molecule is standing in the channel (marker (a)). The translation occurs at the moment the configuration is changing (marker (b)), or when the iodine molecules are lying in the channels (marker (c)). When the iodine molecules are standing, the translation is forbidden due to large repulsive interaction coming from the two ends of the ellipses. During the configuration changing, the translation of the CM is actually induced by the rotation process in which one atom of the iodine molecule keeps in the original wide part and the other atom spans to the neighboring wide part, or from the neighboring wide part to the current wide part. So the distance of the MC is only $c/4$. Contrarily, the size of the short axes of the ellipses (4.3 Å), which is close to twice the van der Waals radius of the iodine molecules, makes it feasible for the iodine molecules to diffuse when they are lying in the channels. It is the way based on which iodine molecules can be introduced into the AEL channels by physical diffusion at high temperature and absorbed in the channels when cooled

to room temperature. The arrows in Figure 7 show the favorable pathways of iodine molecules confined in the AEL channels. It can be seen that the translational barrier is much higher than the rotational barrier of the standing molecules. The standing molecules prefer rotating to lie along the channels to lower the potential energies first and then diffuse along the channels or rotate back and forward to the standing states again.

## 4. Conclusions

The molecular dynamics simulations with a canonical ensemble have been used to study the structures and dynamics of the iodine molecules confined in the $AlPO_4$-11 channels at $T =$ 300 K. We found that the iodine molecules in the AEL channels are effectively restricted in the (101) planes with only two favorite orientations: lying along the channels and standing along the major axes of the ellipses. We attribute these configurations to the shape of the channels, which are not only elliptical but also alternate between wide parts and narrow parts. In addition, the structures of the iodine molecules are loading dependent. With the increase of loading level, the iodine molecules change from vapor phase to single molecular chains and molecular ribbon sheets dominant, in which all the iodine molecules are parallel and equally distributed with a distance of *c*/2. The potential energy surface and the dynamics of the simulations show that the standing iodine molecules in the channels are well confined. They can diffuse along the channels only after overcoming the rotational barriers to become lying molecules. Thus, the iodine molecules in the ribbon sheets are fixed without rotational and translational motion. The iodine molecules within such constraint would be a promising candidate for future metrology.

**Acknowledgment.** This research was supported by Hong Kong CERGC Grants of 602807, 603108, 604210 and HKUST RPC 06/07.SC.06. J.P.Z. thanks the NSFC (50902096) and Guangdong Natural Science Foundation (2008270) for financial support.

**Supporting Information Available:** Fractional coordinates of the AEL crystal measured from single crystal XRD, sample preparation, and optical images of AEL with different loading of iodine molecules. This material is available free of charge via the Internet at http://pubs.acs.org.

## References and Notes

(1) Li, I. L.; Zhai, J. P.; Launois, P.; Ruan, S. C.; Tang, Z. K. *J. Am. Chem. Soc.* **2005**, *127*, 16111–16119.
(2) Wang, N.; Tang, Z. K.; Li, G. D.; Chen, J. S. *Nature* **2000**, *408*, 50–51.
(3) Guan, L. H.; Suenaga, K.; Okubo, S.; Okazaki, T.; lijima, S. *J. Am. Chem. Soc.* **2008**, *130*, 2162–2163.
(4) Ozin, G. A. *Adv. Mater.* **1992**, *4*, 612–649.
(5) Angell, C. A. *Science* **2008**, *319*, 582–587.
(6) Hummer, G.; Rasaiah, J. C.; Noworyta, J. P. *Nature* **2001**, *414*, 188–190.
(7) Hertzsch, T.; Budde, F.; Weber, E.; Hulliger, J. *Angew.Chem. Int. Ed.* **2002**, *41*, 2281–2284.
(8) Tang, Z. K.; Zhang, L. Y.; Wang, N.; Zhang, X. X.; Wen, G. H.; Li, G. D.; Wang, J. N.; Chan, C. T.; Sheng, P. *Science* **2001**, *292*, 2462–2465.
(9) Lortz, R.; Zhang, Q. C.; Shi, W.; Ye, J. T.; Qiu, C. Y.; Wang, Z.; He, H. T.; Sheng, P.; Qian, T. Z.; Tang, Z. K.; Wang, N.; Zhang, X. X.; Wang, J. N.; Chan, C. T. *Proc. Natl. Acad. Sci. U.S.A.* **2009**, *106*, 7299–7303.
(10) Wirnsberger, G.; Fritzer, H. P.; Popitsch, A.; Goor, G. V. D.; Behrens, P. *Angew. Chem., Int. Ed. Engl.* **1996**, *35*, 2777–2779.
(11) Petkov, V.; Billinge, S. J. L.; Vogt, T.; Ichimura, A. S.; Dye, J. L. *Phys. Rev. Lett.* **2002**, *89*, 075502.
(12) Fan, X.; Dickey, E. C.; Eklund, P. C.; Williams, K. A.; Grigorian, L.; Buczko, R.; Pantelides, S. T.; Pennycook, S. J. *Phys. Rev. Lett.* **2000**, *84*, 4621–4624.
(13) Guan, L. H.; Suenaga, K.; Shi, Z. J.; Gu, Z. N.; Lijima, S. *Nano Lett.* **2007**, *7*, 1532–1535.
(14) Gerstenkorn, S.; Luc, P. *J. Phys. (Paris)* **1985**, *46*, 867–881.
(15) Razet, A.; Picard, S. *Metrologia* **1996**, *33*, 19–27.
(16) Zhang, J.; Lu, Z. H.; Wang, L. J. *Appl. Opt.* **2009**, *29*, 5629–5635.
(17) Rabinowitch, E.; Wood, W. C. *J. Chem. Phys.* **1936**, *4*, 358–362.
(18) Lessinger, L. *J. Chem. Educ.* **1994**, *71*, 388–391.
(19) Yoon, T. H.; Ye, J.; Hall, J. L.; Chartier, J. M. *Appl. Phys. B: Lasers Opt.* **2001**, *72*, 221–226.
(20) Goncharov, A.; Amy-Klein, A.; Lopez, O.; Burck, F. Du.; Chardonnet, C. *Appl. Phys. B: Lasers Opt.* **2004**, *78*, 725–731.
(21) Nevsky, A. Y.; Holzwarth, R.; Reichert, J.; Udem, Th.; Hänsch, T. W.; von Zanthier, J.; Walther, H.; Schnatz, H.; Riehle, F.; Pokasov, P. V.; Skvortsov, M. N.; Bagayev, S. N. *Opt. Commun.* **2001**, *192*, 263–272.
(22) Ye, J.; Ma, L. S.; Hall, J. L. *Phys. Rev. Lett.* **2001**, *87*, 270801.
(23) Zhai, J. P.; Li, I. L.; Ruan, S. C.; Lee, H. F.; Tang, Z. K. *Appl. Phys. Lett.* **2008**, *92*, 043117.
(24) Zhai, J. P.; Lee, H. F.; Li, I. L.; Ruan, S. C.; Tang, Z. K. *Nanotechnology* **2008**, *19*, 175604.
(25) Smit, B.; Maesen, T. L. M. *Chem. Rev.* **2008**, *108*, 4125–4184.
(26) Catlow, C. R. A.; van Santen, R. A.; Smit, B. *Computer Modelling of Microporous Materials*; Elsevier Academic Press: London, 2004.
(27) Burchart, E. D. V.; Bekkum, H. V.; Graaf, B. V. D. *J. Chem. Soc., Faraday Trans.* **1992**, *88*, 2761–2769.
(28) Rappé, A. K.; Casewit, C. J.; Colwell, K. S.; Goddard, W. A., III; Skiff, W. M. *J. Am. Chem. Soc.* **1992**, *114*, 10024–10035.
(29) Allen, M. P.; Tildesley, D. J. *Computer Simulation of Liquids*; Oxford University Press: New York, 1989.
(30) Morse, P. M. *Phys. Rev.* **1929**, *34*, 57–64.
(31) Verma, D. R. *J. Chem. Phys.* **1960**, *32*, 738–749.
(32) Plimpton, S. *J. Comput. Phys.* **1995**, *117*, 1–19.
(33) Fang, H. P.; Wan, R. Z.; Gong, X. J.; Lu, H. J.; Li, S. Y. *J. Phys. D: Appl. Phys.* **2008**, *41*, 103002.
(34) van Bolhuis, F.; Koster, P. B.; Migchelsen, T. *Acta Crystallogr.* **1967**, *23*, 90–91.
(35) Ibberson, R. M.; Moze, O.; Petrillo, C. *Mol. Phys.* **1992**, *76*, 395–403.
(36) Lide, D. R. *CRC: The handbook of chemistry and physics*, 84th ed.; CRC Press: Boca Raton, FL, 2006.

JP1076615